Proceedings of ASME Turbo Expo 2017: Turbomachinery Technical Conference and Exposition
GT2017
June 26-30, 2017, Charlotte, NC, USA

GT2017-64616

Effect of Internal Crossflow Velocity on Film Cooling Effectiveness – Part I: Axial Shaped Holes

John W. McClintic, Joshua B. Anderson, and David G. Bogard
The University of Texas at Austin
Austin, Texas, USA

Thomas E. Dyson
GE Global Research
Niskayuna, New York, USA

Zachary D. Webster
GE Aviation
Evendale, Ohio, USA

ABSTRACT

The effect of feeding shaped film cooling holes with an internal crossflow is not well understood. Previous studies have shown internal crossflow reduces film cooling effectiveness from axial shaped holes, but little is known about the mechanisms governing this effect. It was recently shown that the crossflow-to-mainstream velocity ratio is important, but only a few of these crossflow velocity ratios have been studied. This effect is of concern because gas turbine blades typically feature internal passages that feed film cooling holes in this manner. In this study, film cooling effectiveness was measured for a single row of axial shaped cooling holes fed by an internal crossflow with crossflow-to-mainstream velocity ratio varying from 0.2-0.6 and jet-to-mainstream velocity ratios varying from 0.3-1.7. Experiments were conducted in a low speed flat plate facility at coolant-to-mainstream density ratios of 1.2 and 1.8. It was found that film cooling effectiveness was highly sensitive to crossflow velocity at higher injection rates, while it was much less sensitive at lower injection rates. Analysis of the jet shape and lateral spreading found that certain jet characteristic parameters scale well with the crossflow-to-coolant jet velocity ratio, demonstrating that the crossflow effect is governed by how coolant enters the film cooling holes.

INTRODUCTION

GAS TURBINE FILM COOLING

It is necessary in modern gas turbine engines, where temperatures commonly exceed the allowable metal temperature for hot gas path components, to actively cool these components utilizing relatively cool air supplied by the high pressure compressor. This cool air is routed beneath surfaces exposed to the hot combustion products through internal passages that are designed to enhance the heat transfer between the cool internal air and the underside of the exposed surface. For high heat load components, it is often necessary to employ film cooling, wherein the cool gas is ejected through discrete holes in the cooled surface such that a protective layer of cool air forms between the part and the hot combustion products.

Ultimately, the goal of any cooling design aims to minimize the surface temperature of the part, T_m, normalized as an overall cooling effectiveness:

$$\varphi \equiv \frac{T_\infty - T_m}{T_\infty - T_c} \tag{1}$$

However, φ includes both the effects of internal convective cooling and external film cooling and consequently does not allow for the independent analysis of each. Therefore, film cooling performance is typically evaluated in terms of how it affects the important external heat transfer parameters – namely the external driving temperature and heat transfer coefficient. The driving temperature for heat transfer is generally considered to be the adiabatic wall temperature, T_{aw}, and is normalized as adiabatic or film cooling effectiveness:

$$\eta \equiv \frac{T_\infty - T_{aw}}{T_\infty - T_{c,exit}} \tag{2}$$

The heat transfer coefficient, h_f, is often expressed as a ratio to the heat transfer coefficient without film cooling: h_f/h_0.

It is important to understand how these external heat transfer parameters ultimately affect the metal temperature. A simple one-dimensional analysis, assuming a wall of thickness t and thermal conductivity k gives the following:

$$q_f'' = h_f(T_{aw} - T_m) = \frac{T_m - T_c}{t/k - 1/h_c} \tag{3}$$

$$\varphi = \frac{1 - \chi\eta}{1 + Bi + h_f/h_c} + \chi\eta \tag{4}$$

where:

$$\chi \equiv \frac{T_\infty - T_{c,exit}}{T_\infty - T_c} \tag{5}$$

$$Bi \equiv \frac{h_f t}{k} \tag{6}$$

Equation 4 shows how adiabatic effectiveness and the external and internal heat transfer coefficients affect the design parameter of interest, overall effectiveness. This analysis is especially relevant when considering how the internal coolant feed affects the external film cooling performance.

INTERNAL CROSSFLOW EFFECTS

The geometry of interest for this study is the laidback fan-shaped film cooling hole proposed by Schroeder and Thole [1], dubbed the '7-7-7' hole for its 7° forward and lateral expansion angles. Anderson *et al.* [2] found that the performance of this hole scaled best with the coolant-to-mainstream velocity ratio, *VR*, and had a peak film cooling effectiveness at $VR = 1.0$. Boyd *et al.* [3] measured the heat transfer coefficient augmentation for this hole and found that it also scaled best with *VR* and was in most cases, close to unity ($h_f/h_0 \approx 1.0$).

The previously mentioned studies examined film cooling holes fed by a quiescent plenum, which does not represent a typical manner of feeding holes in engine components. Film cooling holes on early stage blades are often fed by internal serpentine channels that run perpendicular to the direction of the overflowing hot mainstream. Flow of this orientation will be hereafter termed "internal crossflow" and is the focus of this study. Much of the available data in the literature regarding shaped film cooling holes fed by an internal crossflow is contained in a few studies performed at Universität Karlsruhe. Although these studies only used a single hole, and measurements were made for only a relatively short distance downstream ($x/d = 8$ to 12), they provide useful insights into this matter. These studies were performed at engine-realistic Mach numbers ($Ma_c = 0.0$-0.6 and $Ma_\infty = 0.3$) and primarily for wide-angle diffuser holes ($\beta = 14°$). The following is a summary of their results regarding how internal crossflow affects adiabatic effectiveness, jet characteristics, and discharge coefficients.

In contrast to cylindrical holes for which internal crossflows improve adiabatic effectiveness for higher blowing ratios [4], for shaped holes, internal crossflows generally degrade performance. Gritsch *et al* [4] found this to be the case for both fan-shaped (FS) and laidback fan-shaped (LFS) holes for crossflow Mach numbers of $Ma_c = 0.3$ and 0.6 and blowing ratios of $M = 0.5$-2.0. Similar observations were made in two studies by Saumweber and Schulz [5, 6]. The effect of increasing crossflow velocity was not as clear. For the FS and LFS geometries of [4], increasing Ma_c from 0.3 to 0.6 generally reduced adiabatic effectiveness, although the effect was small for $M < 1$ for FS holes and for $M > 1.5$ for LFS holes. In [5], a range of $Ma_c = 0.1$-0.6 was tested at $M = 1.0$ and it was found that the effectiveness was not strongly affected by varying Ma_c over that range. In [6], the geometry of FS holes was varied by changing β, α, and L/d. FS holes with narrower diffusion angles ($\beta = 6°$) were found to have reduced effectiveness when Ma_c increased from 0.3 to 0.5 for $M = 1.5$ and increased effectiveness for the same change in Ma_c when $M = 2.5$. There was a similar lack of a clear effect of crossflow velocity on adiabatic effectiveness for varied α and L/d.

The degradation of adiabatic effectiveness in the aforementioned studies corresponded to jet profiles that were asymmetric and biased toward one side of the diffuser. In [4], the jets from $\beta = 14°$ FS holes favored the leeward side of the diffuser relative to the crossflow direction for $M = 0.5$-2.0 and $Ma_c = 0.3$ and 0.5. The LFS holes, on the other hand were typically biased toward the windward side of the diffuser, with the exception of $Ma_c = 0.6$, $M = 0.5$ which was biased toward the leeward side. In [5], the same FS holes were tested over a slightly greater range of Ma_c and M and it was found that the biasing switched to the leeward side at an increased blowing ratio of $M = 2.5$ and at a decreased crossflow velocity of $Ma_c = 0.1$. In [6], the $\beta = 6°$ FS holes tended to bias toward the leeward side of the hole for $Ma_c = 0.3$ and 0.6 and $M = 0.5$-2.5 except for $Ma_c = 0.6$ and $M = 0.5$ when the biasing switched to the windward side, which was a different result from what was seen for the $\beta = 14°$ FS holes in [5]. It was also found that changing α and L/d affected the direction of bias in the diffuser. Saumweber and Schulz [6] used a RANS simulation of flow in the hole to predict that crossflow induced a very strong swirl in the hole that caused a rotation of the jet passing through the hole. The number of rotations, which could be affected by the crossflow rate, injection rate, and hole geometry could explain why the bias was different for the varying conditions tested. Their predictions are similar to those of Kohli and Thole [7] who also predicted a strong swirl in holes fed by crossflow.

A study by Gritsch *et al* [8] showed that crossflow reduces the discharge coefficient for the same FS and LFS holes as [4] fed by an internal crossflow. It was shown that the effect of going from a FS to a LFS hole was small compared to the effect of increasing Ma_c from 0.0 to 0.6. Similarly, increasing Ma_∞ from 0.0 to 0.55 had little effect relative to that of the internal crossflow effect. They found that by normalizing C_d by $C_{d,plenum}$ (without crossflow) at constant pressure ratio, and scaling flow rate by the jet-to-crossflow momentum flux ratio, the data collapsed well – almost to within uncertainty.

More recently, a study in this laboratory by Wilkes *et al* [9] tested crossflow-fed 7-7-7 holes at low Mach number and at two different scales in order to isolate the effects of the internal crossflow-to-mainstream velocity ratio, VR_c, from those of the internal crossflow Reynolds number, Re_c. For this study the channel Reynolds number was varied from $Re_c = 35{,}000$ to 57,000; and the channel velocity ratio was varied from $VR_c = 0.35$ to 0.63. All cases with internal crossflow were found to have significantly decreased adiabatic effectiveness relative to plenum fed holes. They also found that the effectiveness of the film cooling holes was relatively insensitive to changes in Re_c, but was sensitive to changes VR_c. Based on the parameters provided in [4, 5, 6], the internal coolant flow Mach number range of $Ma_c = 0.1$-0.6 used in these studies corresponds to a range of velocity ratios $VR_c = 0.25$-1.5. Since the hole geometries used in these studies were significantly different than that used by Wilkes *et al* [9], meaningful comparisons between these studies are difficult.

PRESENT STUDY

Previous studies found that the decreased performance that occurs with shaped holes fed with internal crossflow occurs due to biasing within the diffuser. The data present in the literature, however, is not as yet sufficient to draw clear conclusions about how injection rate and crossflow velocity interact to produce this effect. Furthermore, the crossflow effect has only been tested for a few geometries. For this study, the 7-7-7 shaped hole (narrow-angle laidback fan-shaped hole) used by [1,2,3,9] was tested. This geometry has a forward expansion that starts deeper in the hole than the studies at Karlsruhe. A wide range of crossflow-to-mainstream velocity ratios, VR_c = 0.2-0.6, and injection rates, VR = 0.3-1.7, were tested in this study using two different density ratios, DR = 1.2 and 1.8. The wider range of parameters allows for analysis of jet parameters that are important for understanding how crossflow affects film cooling. A similar analysis was performed in Part II of this study [10] for compound angle shaped film cooling holes.

NOMENCLATURE

Bi	Biot number
C_d	discharge coefficient
d	film cooling hole diameter
d_H	hydraulic diameter
DR	density ratio ρ_c/ρ_∞
f	friction factor for Gnielinski's formula
H	boundary layer shape factor
h	heat transfer coefficient
k	thermal conductivity
L	film cooling hole length
M	blowing ratio $\rho_j U_j/\rho_\infty U_\infty$
$\dot{m}$	mass flow rate
Ma	Mach number
Nu	Nusselt number
p	film cooling hole pitch, pressure
Pr	Prandtl number
q''	heat flux
R	ideal gas constant for air
Re	Reynolds number
r_x	extraction ratio $\dot{m}_{film}/\dot{m}_{channel}$
S	jet skew
s	equivalent slot width $\pi d_h^2/p$
t	wall thickness
T	temperature
Tu	turbulence intensity $\sqrt{\overline{u'^2}}/\overline{U}$
U	velocity
VR	velocity ratio (without subscript: U_j/U_∞)
W	jet width
x	stream-wise coordinate measured from downstream edge of cooling hole
y	wall-normal coordinate measured from the wall
z	span-wise coordinate

GREEK

α	cooling hole injection angle
β	cooling hole lateral expansion angle
δ	boundary layer thickness, uncertainty
δ^*	boundary layer displacement thickness
φ	overall cooling effectiveness
γ	specific heat ratio, forward expansion angle
η	adiabatic effectiveness
Λ_x	turbulence integral length scale
θ	normalized temperature, boundary layer momentum thickness
ρ	density
χ	coolant warming factor

SUBSCRIPTS, ACCENTS

aw	adiabatic wall
b	bias uncertainty
c	coolant, crossflow
CL	centerline
f	with film cooling
i	hole inlet
j	coolant jet
m	metal
p	precision uncertainty
t	total pressure/temperature
0	without film cooling
∞	mainstream
$\bar{}$	laterally averaged

EXPERIMENTAL FACILITIES AND PROCEDURES

DESCRIPTION OF FACILITIES

Experiments were performed in a low speed, low temperature recirculating wind tunnel at the University of Texas at Austin, a detailed description of which can be found in Anderson *et al* [11] and Wilkes *et al* [9]. Figure 1 shows a schematic of the test section, configured to model flow over a flat plate with a boundary layer starting at an elliptical leading edge and tripped with a cylindrical rod with a diameter of 3.175 mm, positioned 108 mm upstream of the downstream edge of the film cooling holes (x = 0). Relevant mainstream flow parameters are given in Table 1.

Flow was supplied to the film cooling holes through a channel installed below the test coupon and oriented perpendicular to the mainstream flow. The channel was sufficiently long such that the internal channel flow was fully developed before it reached the first film cooling hole. The cross-section of the channel is shown in Figure 1. The film cooling geometry tested in this study was the 7-7-7 hole geometry [1] shown in Figure 2. A single row of eight film cooling holes was machined into a coupon made from polyurethane foam (General Plastics Last-a-Foam R-3315) which had a thermal conductivity of k = 0.044 W/(m·K), suitable for simulating an adiabatic surface. The diameter of the metering (cylindrical) section of the hole was 4 mm and the holes were spaced at a pitch of p/d = 6. This was the same test coupon used in Wilkes *et al* [9].

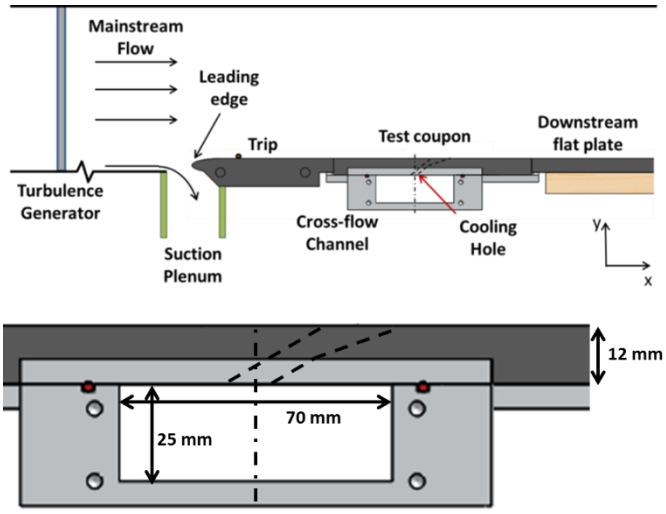

Figure 1: Schematic of test section and channel

Table 1: Mainstream Parameters

Parameter	***Value***
Cooling Hole Diameter, d	4.0 mm
Mainstream Temp, T_∞	310 K
Mainstream Velocity, U_∞	25 m/s
Mainstream Turbulence Intensity, Tu	4.8%
Turbulence Integral Length Scale, Λ_x/d	2.5
Approach Boundary Layer Thickness, δ/d	2.9
Boundary Layer Displacement Thickness, δ^*/d	0.36
Boundary Layer Momentum Thickness, θ/d	0.27
Boundary Layer Shape Factor, H	1.33
Approach Reynolds Number, Re_d	6,000

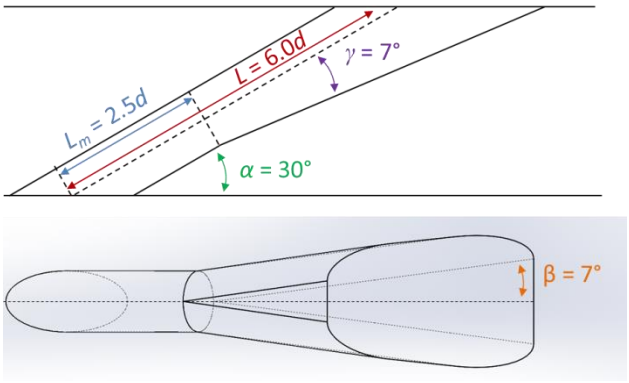

Figure 2: 7-7-7 film cooling hole geometry

Experiments were conducted at two different density ratios, DR = 1.2 and 1.8. The density ratio at typical engine conditions is $DR \approx 2.0$, but many experimental studies use a lower density ratio due to the ease of performing experiments at these conditions. At each density ratio, channel velocity ratio, VR_c and jet-to-mainstream velocity ratio, VR, were varied over the ranges given in Table 2. Unlike the predecessor to this study, Wilkes *et al* [9], channel Reynolds number, Re_c, was allowed to vary freely because it had been shown to have a minimal effect on film cooling effectiveness. The extraction ratio, r_x, (or the percentage of channel inlet flow that was extracted for film cooling) did not exceed 50% and was typically below 15%. An experiment with holes blocked off and matched VR_c and VR showed that there was a negligible effect of extraction ratio on film cooling for these conditions.

Table 2: Experimental Conditions

Parameter	***DR = 1.2***	***DR = 1.8***
$VR = U_j/U_\infty$	0.3 - 1.7	0.3 - 1.7
$VR_c = U_c/U_\infty$	0.2 - 0.6	0.2 - 0.5
$VR_i = U_c/U_j$	0.1 - 2.1	0.1 – 1.8
$M = \rho_\infty U_\infty/\rho_j U_j$	0.3 - 2.0	0.5 - 3.0
Re_c	15,000 - 45,000	31,000 - 78,000
r_x	3 - 48%	3 - 48%

MEASUREMENT TECHNIQUES

A FLIR model A655sc infrared (IR) camera was used to view the test surface through a zinc-selenide window mounted on top of the test section. The surface was painted with a flat black paint to give it a uniform emissivity. The IR camera was calibrated against thermocouples on the surface, mounted on painted copper plates to ensure a uniform surface temperature for the camera to view. Measurements were made at steady state, requiring approximately two hours for the tunnel to reach thermal equilibrium. The camera was set up to view only the center four holes in order to avoid end-of-row effects due to jet-to-jet interactions in the downstream region or different entrance conditions for the first hole seen by the incoming crossflow.

A pitot-static probe, installed downstream of the leading edge measured the mainstream velocity. Calibrated Type E thermocouples measured temperatures in the test facility. The mainstream temperature was calculated as an average of three thermocouples installed near the inlet of the test section. The coolant temperature was the average of the temperature measured at the inlet and outlet of the coolant channel. The pressure at the inlet and exit of the channel were measured to determine the discharge coefficients for the film cooling holes. The film cooling injection flow rate was calculated as the difference between the mass flow rate entering and exiting the coolant channel. These mass flow rates were measured using obstruction meters (a standard ASME orifice plate for the inlet line and a Venturi meter for the outlet line). The outlet Venturi meter was calibrated against the inlet orifice meter to remove bias errors in the coolant flow rate calculation.

DATA ANALYSIS

Discharge Coefficients

The equation from Gritsch *et al* [8] was used to calculate discharge coefficients through the film cooling holes using the

averaged pressure in the channel and measured static pressure in the test section.

$$C_D = \frac{\dot{m}}{\frac{\pi}{4} d^2 p_{tc} \left(\frac{p_\infty}{p_{tc}}\right)^{(\gamma+1)/2\gamma} \sqrt{\frac{2\gamma}{(\gamma-1)RT_{tc}}\left(\left(\frac{p_{tc}}{p_\infty}\right)^{(\gamma-1)/\gamma} - 1\right)}} \quad (7)$$

Conduction Correction

A finite element method was used to correct the measured surface temperatures to remove conduction effects. The test plate downstream of the film cooling holes was modeled and the measured surface temperature was imposed as the boundary condition at the test surface. The predicted heat flux was then used along with the measured heat transfer coefficient without film cooling, h_0, to determine the adiabatic wall temperature. Note that heat transfer coefficient augmentation was assumed to be $h_f/h_0 = 1.0$ based on the results of Boyd *et al* [3]. The correction was then applied using the equation:

$$T_{aw} = T_{measured} - \frac{q''}{h_f} \quad (8)$$

The conduction correction was not applied in the near-hole region ($x/d < 2$) due to the conduction around the film cooling holes. Details regarding this method are in Klavetter *et al* [12].

Jet Characteristic Parameters

Internal crossflow causes biasing of the coolant within the diffuser, resulting in asymmetric jets that have a location of peak effectiveness that deviates from the geometric centerline of the hole. Four different jet characteristic parameters were used to analyze this effect: jet centerline effectiveness and location, jet width, and jet skew. Figure 3 shows how the first three parameters were determined. The term "centerline effectiveness", or η_{CL}, refers to the peak adiabatic effectiveness of the jet at a given streamwise location, regardless of whether the peak effectiveness level is on the hole geometric centerline. The centerline location, $(z/d)_{CL}$, is the location of η_{CL} relative to the geometric centerline. Note that the positive z axis is aligned with the direction of internal crossflow. The jet width, W, is defined as the spanwise distance between the points on either side of the jet where $\eta = 0.5\eta_{CL}$, or $W/d = (z/d)_{-1} - (z/d)_{+1}$. Jet width is defined in this manner so as to evaluate jet width independently of the centerline effectiveness. The jet skew, S, quantifies the asymmetry of the jet about the peak effectiveness location and is defined as follows:

$$S \equiv 1 - \frac{2\int_{(z/d)_{-1}}^{(z/d)_{CL}} \eta d(z/d)}{\int_{(z/d)_{-1}}^{(z/d)_{+1}} \eta d(z/d)} \quad (9)$$

A skew of $S = 0$ is therefore a perfectly symmetric jet profile, while a positive skew indicates a jet that is more effective on the positive side of $(z/d)_{CL}$ while the reverse is true for a jet with negative skew. The maximum absolute value of skew is $|S| = 1$.

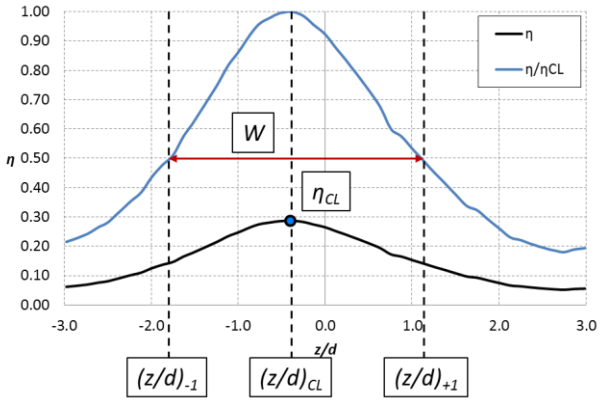

Figure 3: Jet characteristic parameters – sample η profile at $x/d = 10$

Predicted Overall Effectiveness

Using Eqn. 4, a simple one-dimensional model was used to predict overall effectiveness using the measured adiabatic effectiveness and assumptions about the internal and external heat transfer coefficients. Similarly to the conduction correction, it was assumed that heat transfer coefficient augmentation, $h_f/h_0 = 1.0$. The internal heat transfer coefficient was calculated from Gnielinski's formula for turbulent internal flow:

$$Nu_D = \frac{h_c d_H}{k_c} = \frac{(f/8)(Re_c - 1000)Pr}{1 + 12.7(f/8)^{1/2}(Pr^{2/3} - 1)} \quad (10)$$

$$f = (0.79\ln(Re_c) - 1.64)^{-2} \quad (11)$$

It was furthermore assumed that the coolant warming factor, $\chi = 0.9$. This assumption takes into account the warming through the film cooling holes. A Biot number, defined in Eqn. 6, of $Bi = 0.8$ was chosen to be representative of engine conditions where it is expected that the Biot number ranges from $Bi = 0.1 - 1.0$ [13]. This model was not expected to predict overall effectiveness that closely matches engine conditions; rather, it evaluated the effect of varying VR_c, taking both external and internal effects into account.

REPEATABILITY AND UNCERTAINTY

Test-to-test repeatability was confirmed for a number of cases. Figure 4 shows the test-to-test repeatability of laterally averaged effectiveness for $DR = 1.2$ and $VR_c = 0.3$. The repeatability of the experiment was $\delta\eta_R = \pm 0.004$.

Uncertainty was estimated using the sequential perturbation method of Moffat *et al* [14]. The precision uncertainty of effectiveness values presented in this study was estimated to be $\delta\eta_P = \pm 0.005$ for $DR = 1.2$ and $\delta\eta_P = \pm 0.011$ for $DR = 1.8$. The higher uncertainty for $DR = 1.8$ was due to increased jet-to-jet variation. The higher jet variation was presumed to be an effect of frost forming in and around the film cooling holes. Care was taken to continually inspect the film cooling holes throughout the experiment and to defrost them by

forcing ingestion into the holes. The results for the DR = 1.8 condition were filtered such that only conditions where the jet-to-jet variation was within ±0.01 are presented for the purposes of this study. The bias uncertainty in adiabatic effectiveness was $\delta\eta_b = \pm 0.016$ for DR = 1.2 and $\delta\eta_b = \pm 0.012$ for DR = 1.8, and were primarily a result of the bias uncertainty in the camera calibration and the flow rate measurement. The bias and precision uncertainties in velocity ratio were $\delta(VR)_b = \pm 0.03$ and $\delta(VR)_p = \pm 0.010$ respectively. The bias and precision uncertainties for the crossflow velocity ratio were $\delta(VR_c)_b = \pm 0.005$ and $\delta(VR_c)_p = \pm 0.001$ respectively.

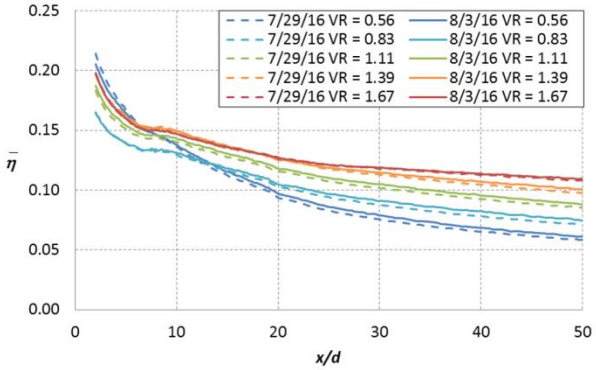

Figure 4: Test-to-test repeatability of laterally averaged effectiveness, DR = 1.2, VR_c = 0.3

RESULTS AND DISCUSSION

Adiabatic effectiveness and discharge coefficients were measured for a single row of 7-7-7 laidback fan-shaped holes for varying density ratio, DR, jet-to-mainstream velocity ratio, VR, and internal crossflow-to-mainstream velocity ratio, VR_c. The aim of these measurements was to provide data over a wider range of VR_c and x/d than has previously been studied in order to better understand how internal crossflow affects film cooling effectiveness.

EFFECT OF DENSITY RATIO

A number of studies have endeavored to determine which injection parameter best scales effectiveness for varying density ratio. This type of analysis enables scaling between low DR experiments and high DR engine conditions. Most relevantly, Anderson *et al* [2] found that adiabatic effectiveness scaled best with jet-to-mainstream velocity ratio, VR, for plenum-fed 7-7-7 holes. Unlike the findings of Anderson *et al* [2], no single parameter best scaled the adiabatic effectiveness data; however, blowing ratio, M, and VR were found to work well in certain cases. Figure 5 shows laterally averaged effectiveness scaled with both VR and M in the near-hole region (x/d = 10) and further downstream (x/d = 40) for two different crossflow-to-mainstream velocity ratios, VR_c = 0.3 and 0.5. First, the velocity ratio of VR_c = 0.3 had higher laterally averaged effectiveness than VR_c = 0.5 for higher injection rates. This trend was the same for both DR = 1.2 and 1.8 suggesting that important flow physics at DR = 1.8 were preserved at DR = 1.2.

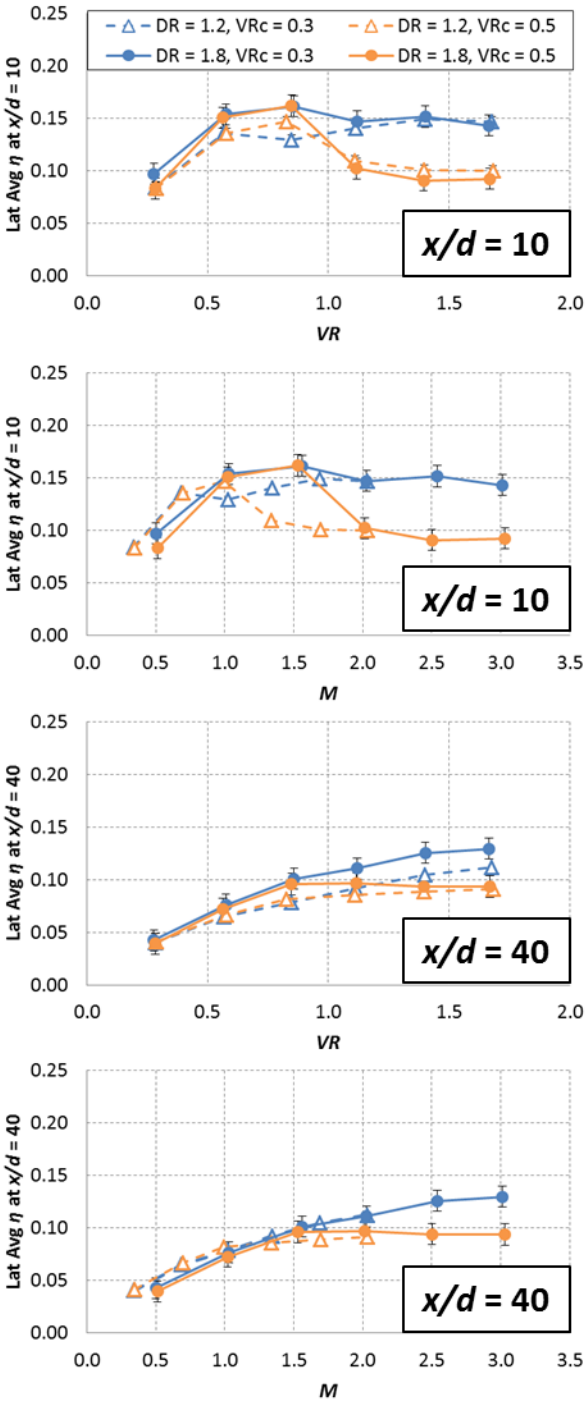

Figure 5: Laterally averaged effectiveness for selected streamwise locations scaled with VR and M

Secondly, VR was the better scaling parameter at x/d = 10, collapsing the data at each VR_c to within uncertainty for all but the low injection rates for VR_c = 0.3. Scaling with M failed to collapse the curves for M = 1.0-2.0 at x/d = 10. The better scaling with VR in the near hole region accounts for turbulent mixing in the shear layers as the jet exits the hole. However,

further downstream at x/d = 40, both crossflow velocity ratios collapsed within uncertainty when scaled with M. For VR_c = 0.5, the effectiveness also appears to collapse well with VR at x/d = 40, but the same cannot be said for VR_c = 0.3. Effectiveness in the far downstream region was therefore most affected by the mass flux of the coolant leaving the hole.

Laterally averaged η was scaled with x/Ms, where s is an equivalent slot width. Scaling with x/Ms is expected to collapse the laterally averaged curves for jets that have not separated from the wall because it takes into account the added coolant mass above the wall by scaling with M. However, for VR_c = 0.5, there was a much larger reduction in effectiveness when VR increased to 1.1 for both density ratios. This result is interesting, especially given that scaling with M is inherent in the x/Ms scaling, yet the injection rate at which the drop-off in effectiveness occurred scaled with VR. The reduction in effectiveness at higher VR shows that the higher crossflow velocity was altering the manner in which the jets exit the hole and therefore less coolant remains close to the wall to protect it from the overflowing hot mainstream gas.

It is evident that the density ratio had a weak but measurable effect on film cooling from 7-7-7 holes fed by an internal crossflow. Given that important trends were preserved between the two density ratios, the remaining results of this paper will be presented for DR = 1.2 because more data was acquired at that density ratio and at higher accuracy. All conclusions that can be drawn from the DR = 1.2 data can similarly be drawn from the DR = 1.8 data.

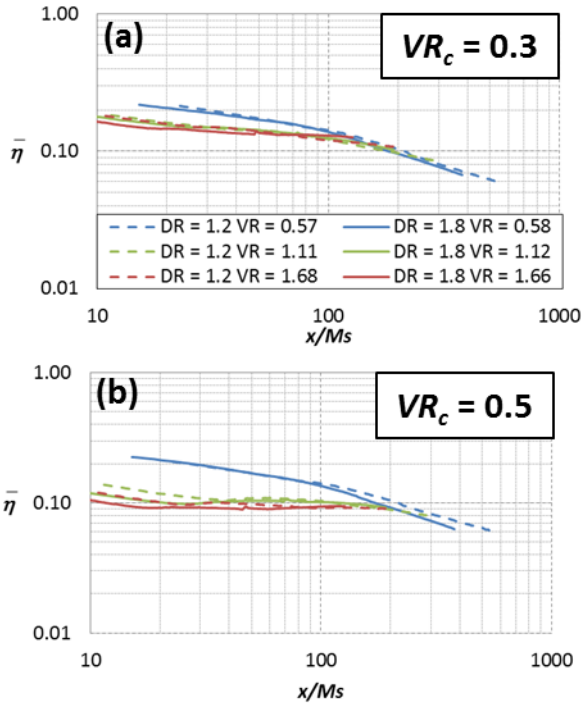

Figure 6: Laterally averaged effectiveness scaled with x/Ms for (a) VR_c = 0.3 (b) VR_c = 0.5

EFFECT OF CHANNEL VELOCITY RATIO

Effect on Adiabatic Effectiveness

Little is known about the effect of increasing VR_c on adiabatic effectiveness. Saumweber and Schulz [6] showed that the effect is geometry dependent for fan-shaped holes. The geometry for this study was a laidback fan-shaped hole, which, based on the results of Gritsch *et al* [4], is expected to behave differently than a fan-shaped hole with no laidback angle in terms of both effectiveness and biasing direction.

In this study, it was found that for axial 7-7-7 laidback fan-shaped holes, increasing crossflow velocity caused a reduction in effectiveness at higher injection rates. Figure 7 compares the spatially averaged effectiveness for all VR_c tested. The trend of decreasing η with increasing VR_c applied for $VR \geq 1.4$. For $VR < 1.0$, there was very little effect of increasing crossflow velocity, with the exception of the plenum-fed case, the data for which was measured by Anderson *et al* [2]. The reduction in effectiveness relative to the plenum-fed case at lower VR was consistent with what has been seen in the literature for crossflow-fed shaped holes, but at higher VR, the effectiveness from the plenum-fed holes was lower than the crossflow-fed holes at VR_c = 0.2. While this effect has not been observed in the literature, there is no data available in the literature at $VR_c < 0.4$. A possible explanation for this result is that the plenum-fed holes separated at around VR = 1.0, while the extent of separation for crossflow-fed holes was small at lower VR_c, as indicated by Figure 6 (a). Increasing VR_c also changed the VR at which the peak effectiveness level occurred. The most significant shift in the VR corresponding to peak effectiveness occurred between VR_c = 0.3 and 0.4, where it changed from VR = 1.4 to 0.6.

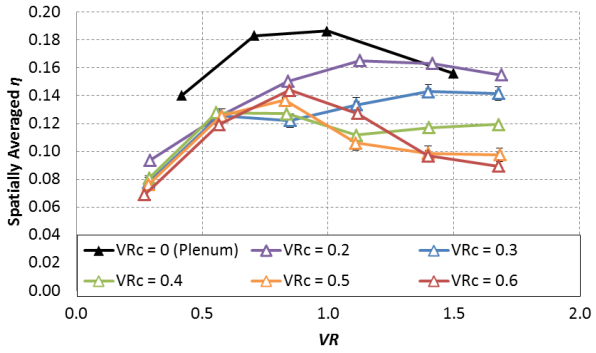

Figure 7: Spatially averaged effectiveness, DR = 1.2, averaged from x/d = 5-20, plenum data from [2]

The degradation in effectiveness due to internal crossflow was influenced by biasing of the jet within the diffuser. Figure 8 shows contours of η (uncorrected η is used here to show the observed temperature profile in the diffuser) for VR = 1.67 at VR_c = 0.2, 0.4, and 0.6. At VR_c = 0.2, the jet profile was nearly symmetric about the hole's geometric centerline, although some biasing in the diffuser was evident. As the crossflow velocity

increased to VR_c = 0.6, the jet was strongly biased toward the windward side of the diffuser, causing an asymmetric jet with spanwise movement in the opposite direction of the internal crossflow. The increased biasing in the hole caused reduced adiabatic effectiveness, likely due to increased mixing of the coolant with the mainstream. The greater degree of biasing at greater VR_c indicates that the higher crossflow velocity resulted in a larger separation region at the hole inlet. Note that the direction of jet bias was the same as Gritsch *et al* [4] for laidback fan-shaped holes, although the holes in that study had a double peak due to having greater lateral expansion angles.

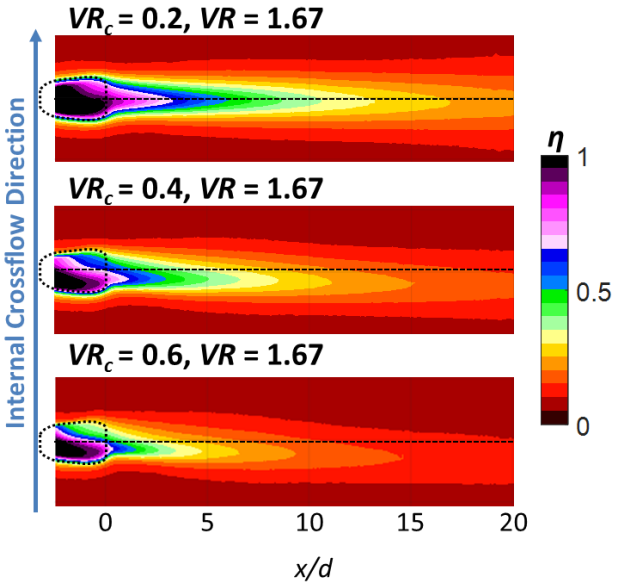

Figure 8: Contours of uncorrected η at VR = 1.67 for VR_c = 0.2, 0.4, and 0.6

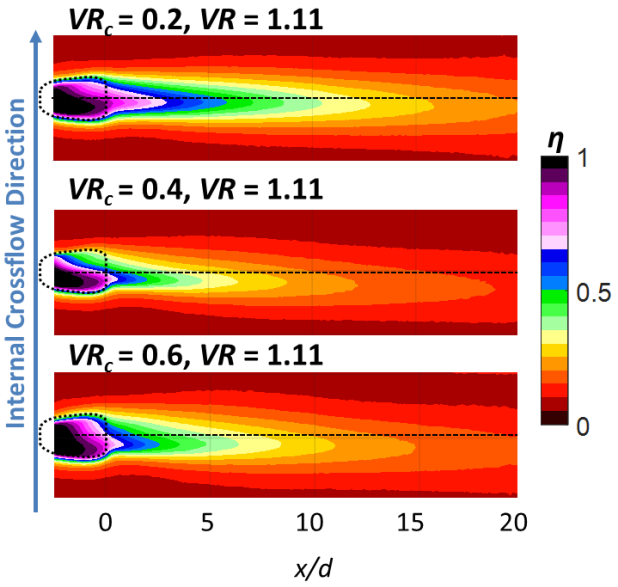

Figure 9: Contours of uncorrected η at VR = 1.11 for VR_c = 0.2, 0.4, and 0.6

The biasing in the diffuser did not always increase with increasing crossflow velocity. Figure 9 shows contours of uncorrected adiabatic effectiveness for VR = 1.11 for the same three crossflow-to-mainstream velocity ratios as for Figure 8. Similar to VR = 1.67, the effectiveness decreased and the diffuser biasing increased when VR_c was increased from 0.2 to 0.4, but when increased from VRc = 0.4 to 0.6, the biasing in the diffuser was reduced and the effectiveness increased.

Effect on Jet Characteristics

Four different jet characteristic parameters were analyzed to quantify the effects of crossflow on the film cooling jet profiles: jet centerline effectiveness, η_{CL}, centerline location, $(z/d)_{CL}$, jet width, W/d, and jet skew, S. Figure 10 shows these four parameters for varying VR_c at VR = 1.11 (corresponding to the contours of Figure 9). Note that η_{CL} does not match between Figures 9 and 10 because the jet parameters were computed using corrected η. The centerline effectiveness (shown in Fig. 10a) was highest for VR_c = 0.2 and decreased with increasing VR_c to a minimum at VR_c = 0.4 and 0.5 and then increased going to VR_c = 0.6. The differences in η_{CL} were most pronounced in the near-hole region and largely disappeared by x/d = 30. The jet centerline location (Fig. 10b) was negative relative to the geometric centerline of the hole for all VR_c at this injection rate. As VR_c increased, $(z/d)_{CL}$ moved further from the geometric centerline until VR_c = 0.5 and then moved back toward the geometric centerline when VR_c was increased to 0.6. The minimum centerline effectiveness corresponded with the maximum jet movement, indicating a link between the extent of jet lateral movement (caused by biasing in the diffuser) and the centerline effectiveness of the jet. This phenomenon was likely driven by increased jet mixing with the mainstream flow as the jet moved laterally and as the biasing in the diffuser became more severe. Also note that going downstream, the jet centerlines tended to move away from the geometric centerline, which was unexpected given that the mainstream flow tends to force film cooling jets to turn in the streamwise direction. It is likely that asymmetrical vortices within the jet, similar to those predicted by Saumweber and Schulz [5] imparted a lateral movement to the jets. The jet width (Fig. 10c), as defined in Figure 3, increased with increasing VR_c up to VR_c = 0.4. Recall that the hole pitch was p/d = 6, which sets the maximum W/d, above which the jets merge and W/d is no longer defined. Increased W/d did not necessarily correlate to the increased lateral movement of the jet, as the jet for VR_c = 0.6, which had little lateral movement, had roughly the same width as VR_c = 0.4 and 0.5, which had more lateral movement. Jet skew (Fig. 10d) was a noisy parameter, but tended to be positive for all VR_c at VR = 1.1. S rapidly decayed to 0 and was negligible by x/d = 15. Positive S means that the jet was more effective on the positive side of its centerline. VR_c = 0.6 had the most skewed jet profile in the near-hole region while VR_c = 0.2 had the least skew near the hole. Even though these two cases had similar jet movement, the VR_c = 0.6 jet was more asymmetric, indicating that the strength of the internal crossflow did more than just bias the jets in the diffuser.

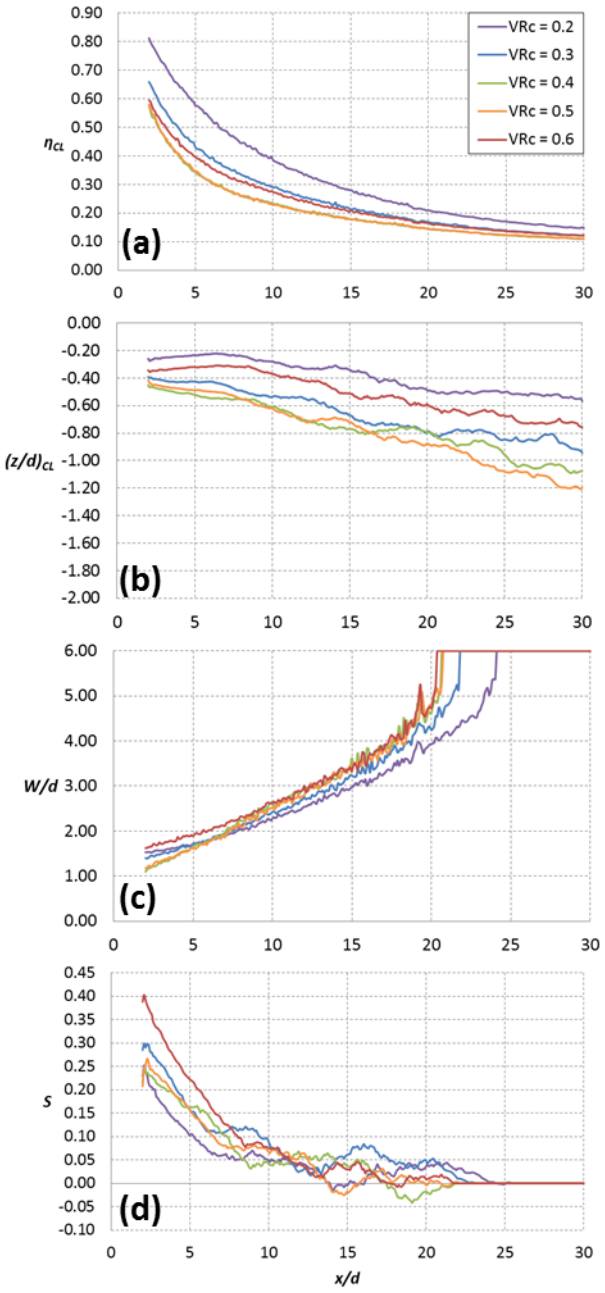

Figure 10: Jet characteristic parameters for *DR* = 1.2, *VR* = 1.11, (a) η_{CL}, (b) $(z/d)_{CL}$, (c) *W/d* (d) *S*

As with adiabatic effectiveness, it was useful to average the jet shape parameters to understand how they were affected by internal crossflow. However, as was shown by the effectiveness and jet shape parameters for VR = 1.11 and 1.67 in Figures 9 and 10, VR_c was not a sufficient parameter to scale the crossflow effects as the effect of increasing VR_c was not consistent across the two injection rates. Instead, the average jet parameters were scaled with the hole inlet velocity ratio, $VR_i = U_c/U_j$. Figure 11 shows jet parameters averaged from x/d = 5-20 scaled with VR_i. For all jet parameters, scaling with VR_i caused most of the averaged values to collapse across the range of VR_c and VR tested in this study. Most interestingly, the local minimum in η_{CL} corresponded with the maximum negative spanwise jet movement as well as a local minimum in jet skew – all occurring at VR_i = 0.4. This result demonstrates that, at least for the 7-7-7 geometry, there was a critical hole inlet velocity ratio that maximized biasing in the diffuser, which resulted in reduced film cooling effectiveness. The value of the critical VR_i, while likely dependent on geometry and other factors not varied in this current study, is likely an important parameter for engine designers to be conscious of when designing the cooling systems in the hot gas path of gas turbine engines. However, it is unclear why a critical VR_i exists. It is almost certainly a result of how the separation region at the hole inlet influences biasing in the diffuser, but the nature of that influence remains unknown and unmeasured. As was shown in Figures 8 and 9, the coolant in the diffuser was biased toward the windward side of the hole relative to the direction of internal crossflow. This result, which is consistent with literature, is counterintuitive in that this is the same side of the hole on which the separation region forms, while most of the coolant would be directed to the leeward side of the hole inlet. Some effect, such as swirling within the hole, or the inability of the jetting coolant on the leeward side of the metering hole to diffuse in the leeward direction when it reaches the diffuser was responsible for biasing the coolant toward the windward side of the diffuser for $VR_i < 1.1$.

The other important inlet velocity ratio is VR_i = 1.1, where the coolant switched from being biased toward the windward side of the diffuser to being biased toward the leeward side of the diffuser. A similar result was seen in Gritsch *et al* [4] for laidback fan-shaped holes at the highest crossflow velocity and the lowest injection rate (which is consistent with a high VR_i). The sign of the average jet skew also changed from positive to negative at VR_i = 1.1, indicating that the skew of the jet was tied to whatever phenomenon governs the biasing of the jet within the diffuser.

There were other notable trends in the average jet parameters shown in Figure 11. Generally, η_{CL} decreased with increasing VR_i, which was primarily a result of VR decreasing with VR_i as well and less coolant being supplied to the holes. The scaling of η_{CL} with VR_i broke down at low VR – the five points on Figure 11 (a) with $\eta_{CL} < 0.15$ were all at VR = 0.28. At these low injection rates, the effectiveness was tied more to the mass flow rate of coolant than to the crossflow effect, although the jet biasing was still affected by VR_i. The jet width did not collapse as cleanly as the other parameters, but tended to increase with increasing VR_i. The most notable deviation from scaling the jet parameters with VR_i is not shown in Figure 11. The average jet skew for VR_c = 0.2 was not plotted because it did not collapse with the rest of the data and obscured the observed trend in Figure 11 (d). The skew for VR_c = 0.2 was closer to S = 0, which is expected given that in the limit as VR_i goes to zero (plenum condition), the skew is also expected to go to zero, so there must be some VR_c at which the scaling of skew with VR_i breaks down.

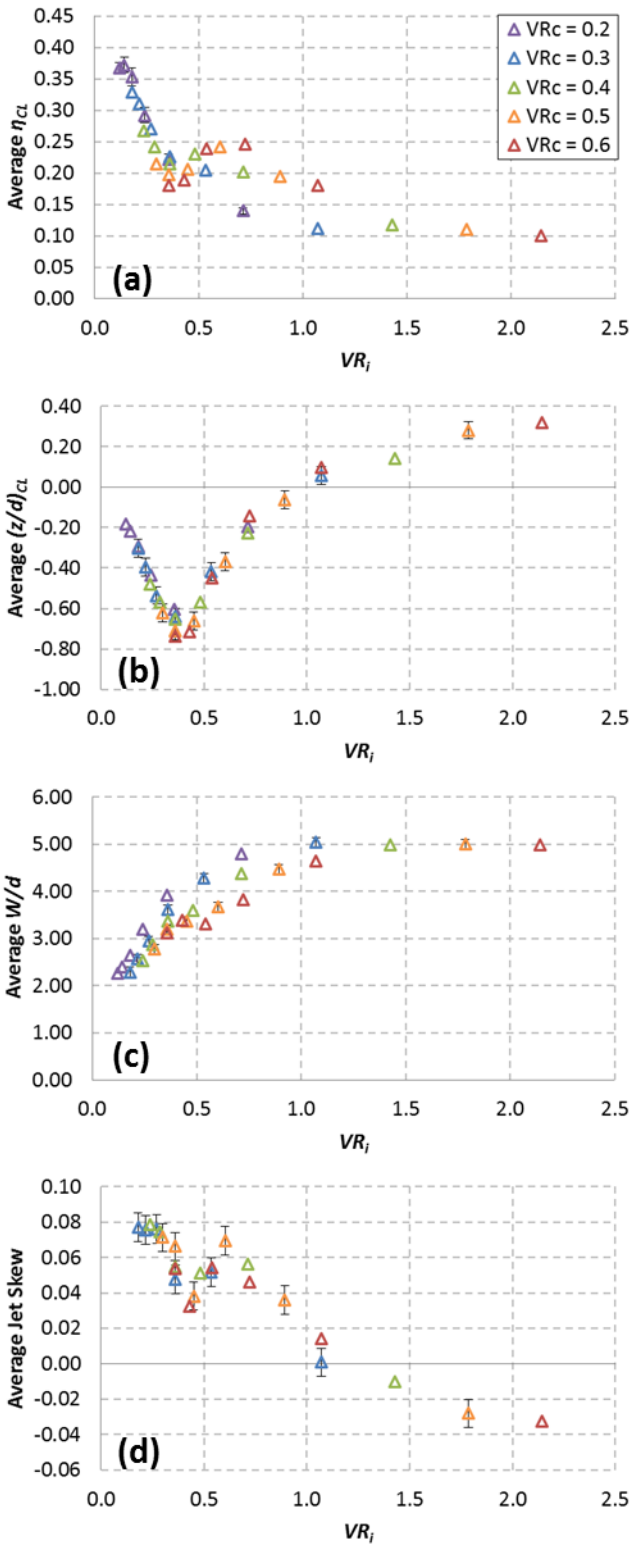

Figure 11: Jet parameters averaged over *x/d* = 5-20, *DR* = 1.2, (a) η_{CL}, (b) $(z/d)_{CL}$, (c) *W/d*, (d) *S*

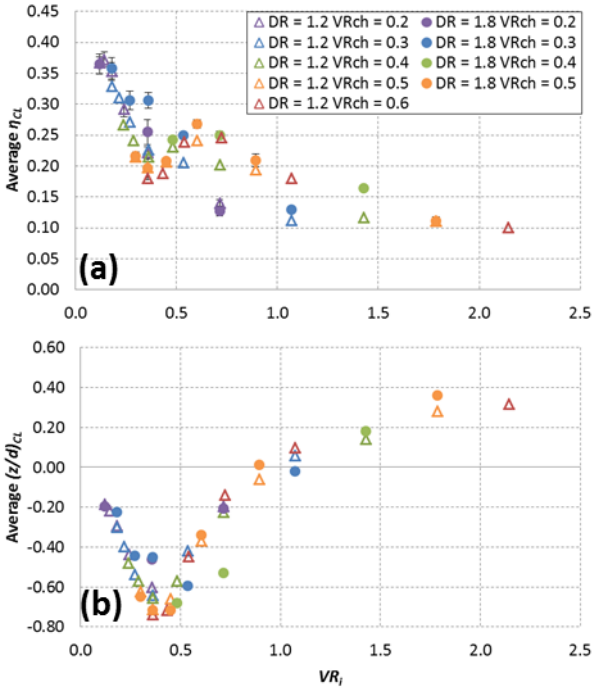

Figure 12: Jet parameters averaged over *x/d* = 5-20, *DR* = 1.2 and 1.8, (a) η_{CL}, (b) $(z/d)_{CL}$

Figure 12 shows that the same trend was observed for *DR* = 1.8 as shown in Figure 11 (a) and (b). This is an important result because it confirms that the flow physics that governed biasing of the jet and the reduction of effectiveness due to crossflow were maintained over the range of *DR* = 1.2 to 1.8.

Effect on Discharge Coefficient

Discharge coefficients were measured for all conditions tested. The discharge coefficient is a useful metric in that it quantifies the losses through the holes and ties the pressure ratio across the hole ($PR = p_{t,c}/p_\infty$) to the flow rate through the hole. It was found that the discharge coefficient scaled well with jet-to-channel velocity ratio. Figure 13 (a) and (b) show discharge coefficients for all five tested velocity ratios plotted against *PR* and U_j/U_c respectively. (Note that $U_j/U_c = 1/VR_i$.) When scaled with pressure ratio, the discharge coefficient decreased with increasing VR_c, which is expected – the higher the crossflow velocity, the more difficult it is for the flow to turn into the hole. This effect was captured when discharge coefficients were scaled with U_j/U_c as the curves for VR_c = 0.3-0.6 collapsed onto a single curve. There was a deviation from this curve for VR_c = 0.2. This result is not surprising considering that as internal crossflow velocity is driven to zero (i.e. the traditional plenum feed), U_j/U_c goes to infinity, but C_d remains a function of pressure ratio across the hole. Thus, at a low enough VR_c (in this case between VR_c = 0.2 and 0.3) the scaling with U_j/U_c must necessarily break down.

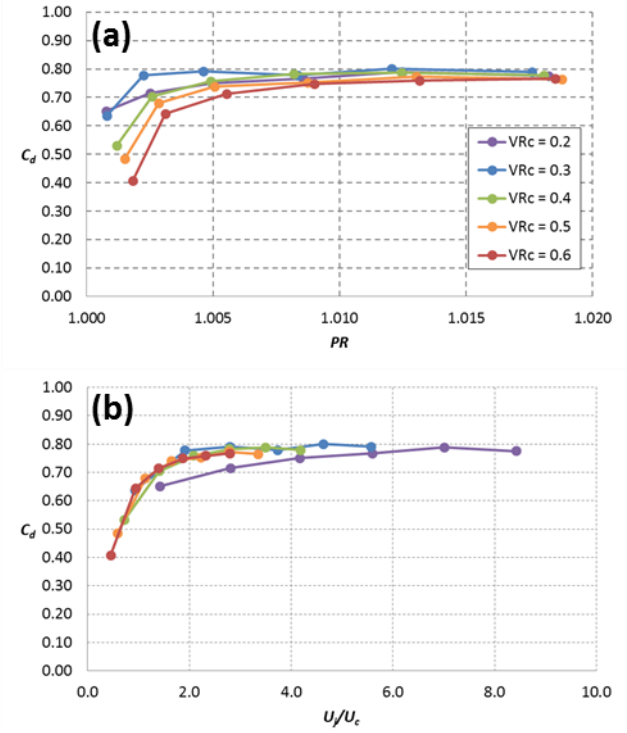

Figure 13: Discharge coefficients for all VR_c tested at DR = 1.2. (a) scaled with PR (b) scaled with U_j/U_c

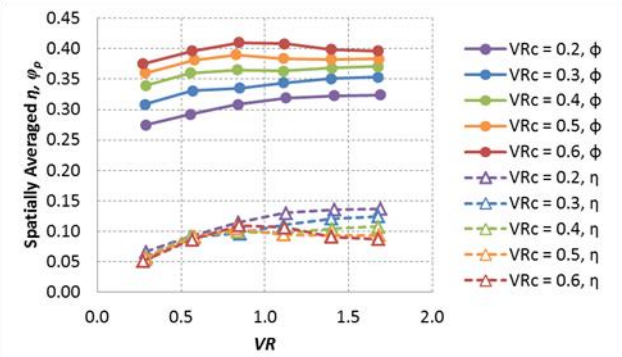

Figure 14: Comparison of predicted φ_p and measured η, spatially averaged from x/d = 5-20, DR = 1.2

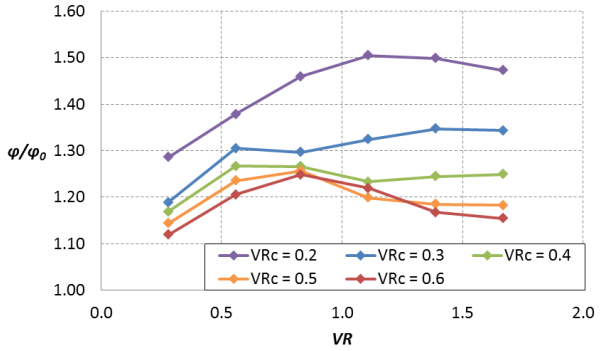

Figure 15: Ratio of spatially averaged (x/d = 5-20) predicted film cooling effectiveness to predicted film cooling effectiveness without film cooling

PREDICTION OF OVERALL EFFECTIVENESS

Because changing the crossflow velocity not only affects the film cooling performance, but also affects the internal cooling of the part, a one-dimensional model (Eqn. 4) was used to predict the overall effectiveness to take both of these effects into account. As shown in Figure 14, the model predicted that the benefit of improving internal cooling by increasing VR_c from 0.2 to 0.6 (and therefore increasing Re_c from 15,000 to 45,000) outweighs the penalty of decreasing film cooling effectiveness. This analysis did not take into account the penalty that higher coolant mass flow rates impose on the efficiency to an engine, so the optimal operating condition is still somewhat unclear. The prediction of overall effectiveness has a number of other uses, however, such as showing how much introducing film cooling improves overall effectiveness over the base condition of an internally cooled part without film cooling, represented by the overall film cooling effectiveness without film cooling, φ_0. Figure 15 plots the ratio of φ_p/φ_0, showing that film cooling is far more critical for parts that are fed by low internal coolant flow rates and therefore have less internal cooling. In this simplified case, introducing film cooling caused up to a 50% increase in overall cooling effectiveness for VR_c = 0.2 and only a 25% increase in φ for VR_c = 0.6.

CONCLUSIONS

Adiabatic effectiveness and discharge coefficients were measured for 7-7-7 axial shaped holes for a range of internal corssflow-to-mainstream velocity ratios of VR_c = 0.2-0.6 and injection rates of VR = 0.3-1.7 at two density ratios: DR = 1.2 and 1.8. The important conclusions from this study are as follows:

- Most of the important physics, including jet centerline effectiveness, jet characteristic parameters, and discharge coefficients scaled with the hole inlet velocity ratio, VR_i. This is the first study to the authors' knowledge to demonstrate the importance of this velocity ratio.
- An examination of jet shape parameters discovered the existence of a critical hole inlet velocity ratio of VR_i = 0.4 at which jet biasing was most extreme resulting in reduced adiabatic effectiveness.
- In general, increased jet biasing tended to result in decreased adiabatic effectiveness.
- Increasing the crossflow-to-mainstream velocity ratio, VR_c, decreased adiabatic effectiveness for VR > 1.1, while at lower injection rates, effectiveness was insensitive to changes in VR_c.

- There was a small effect of changing density ratio from *DR* = 1.8 to 1.2. However, non-dimensional performance parameters were very similar for both density ratios. This result showed that film cooling performance can be reasonably simulated at lower density ratio when scaled appropriately.
- A one-dimensional model was used to predict overall effectiveness. It found that the benefits from increasing internal cooling performance were greater than the accompanying degradation of adiabatic effectiveness due to higher internal crossflow velocity.

While the results of this study are intriguing, there are a number of questions still to be answered regarding the effect of internal crossflow on film cooling effectiveness. Most importantly, in-hole flow physics that govern how the coolant biases in the diffuser of the hole are not well understood. Flow and thermal field measurements near and within the hole are needed to explain these effects. Also, a better understanding of how different shaped hole geometries are affected by internal crossflow is needed.

ACKNOWLEDGMENTS

The authors are grateful for the continued financial and technical support from GE Aviation and GE Global Research.

REFERENCES

[1] Schroeder, R. P. and Thole, K. A., 2014, "Adiabatic Effectiveness Measurements for a Baseline Shaped Film Cooling Hole," ASME Paper No. GT2014-25992.

[2] Anderson, J. B., Boyd, E. J., and Bogard, D. G., 2015, "Experimental Investigation of Coolant-to-Mainstream Scaling Parameters with Cylindrical and Shaped Film Cooling Holes." ASME Paper No. GT2015-43072.

[3] Boyd, E. J., McClintic, J. W., Chavez, K. F., and Bogard, D. G., 2014, "Direct Measurement of Heat Transfer Coefficient Augmentation at Multiple Density Ratios," *J. Turbomach*., **139**, pp. 011005.

[4] Gritsch, M., Schulz, A., and Wittig, S., 2003, "Effect of Internal Coolant Crossflow on the Effectiveness of Shaped Film-Cooling Holes," *J. Turbomach*., **125**, pp. 547-554.

[5] Saumweber, C., and Schulz, A., 2008, "Comparison of the Cooling Performance of Cylindrical and Fan-Shaped Cooling Holes with Special Emphasis on the Effect of Internal Coolant Cross-Flow," ASME paper GT2008-51036, Berlin, Germany.

[6] Saumweber, C. and Schulz, A., 2012, "Effect of Geometry Variations on the Cooling Performance of Fan-Shaped Cooling Holes," *J. Turbomach*., **134**, p.061008.

[7] Kohli, A. and Thole, K. A., 1998, "Entrance Effects on Diffused Film-Cooling Holes," ASME Paper No. 98-GT-402.

[8] Gritsch, M., Saumweber, C., Schulz, A., Wittig, S., and Sharp, E., 2000, "Effect of Internal Coolant Crossflow Orientation on the Discharge Coefficient of Shaped Film-Cooling Holes," *J. Turbomach*., **122**, pp. 146-152.

[9] Wilkes, E. K., Anderson, J. B., McClintic, J. W., and Bogard, D. G., 2016, "An Investigation of Turbine Film Cooling Effectiveness with Shaped Holes and Internal Cross-Flow with Varying Operational Parameters," ASME Paper No. GT2016-56162.

[10] McClintic, J. W., Anderson, J. B., Bogard, D. G., Dyson, T. E., and Webster, Z., 2017, "Effect of Internal Crossflow Velocity on Film Cooling Effectiveness – Part II: Compound Angle Shaped Holes," ASME Paper No. GT2017-64624.

[11] Anderson, J. B., Wilkes, E. K., McClintic, J. W., and Bogard, D. G., "Effects of Freestream Mach Number, Reynolds Number, and Boundary Layer Thickness on Film Cooling Effectiveness of Shaped Holes," ASME Paper No. GT2016-56152.

[12] Klavetter, S. R., McClintic, J. W., Bogard, D. G., Dees, J. E., Laskowski, G. M., and Briggs, R., 2015, "The Effect of Rib Turbulators on Film Cooling Effectiveness of Round Compound Angle Holes Fed by an Internal Cross-Flow," ASME Paper No. GT2015-43947.

[13] Dyson, T. E., McClintic, J. W., Bogard, D. G., and Bradshaw, S. D., 2013, "Adiabatic and Overall Effectiveness for a Fully Cooled Turbine Vane," ASME Paper No. GT2013-94928.

[14] Moffat, R. J., 1985, "Using Uncertainty Analysis in the Planning of an Experiment," *J. Fluids Eng.*, **107**, pp. 173-178.